PRAMANA
— journal of
physics

Vol. 61, No. 1
July 2003
pp. 51–66

Fusion, resonances and scattering in $^{12}C+^{12}C$ reaction

B SAHU, S K AGARWALLA and C S SHASTRY*
Department of Physics, Khallikote College, Berhampur 760 001, India
*Department of Physics, North Eastern Hill University, Shillong 793 022, India
Email: sahu12@sancharnet.in

MS received 12 May 2002; revised 13 January 2003; accepted 21 February 2003

Abstract. The variation of fusion cross-section ($\sigma_{\rm fus}$) with energy in the $^{12}C+^{12}C$ collision is linked to the underlying resonance phenomenon through the behavior of reaction cross-section ($\sigma_{\rm r}$) of which $\sigma_{\rm fus}$ is taken as a part. The calculation of $\sigma_{\rm fus}$ is done through an energy-dependent imaginary potential in the optical model potential (OMP). Through dispersion relation, such an imaginary potential gives rise to energy-dependent real potential which is incorporated in the OMP. In our calculation, a form of potential for the nuclear part which has a soft repulsive in-built core is introduced based on similar works done earlier. The calculated results of $\sigma_{\rm fus}$ are used to explain the oscillatory structure, astrophysical *S*-factor and the decreasing trend at higher energies of the experimental $\sigma_{\rm fus}$ data in the case of $^{12}C+^{12}C$ system with remarkable success. The potential used for fusion calculation is tested for fitting elastic scattering data at some energies and is found good in forward angles. Further improvement of the fitting of these data is obtained by incorporating a coupling potential in the surface region. About twenty resonances are observed in our calculation in the specific partial waves and some of them are found close to the experimentally identified resonances in $^{12}C+^{12}C$ reaction. Thus, we provide an integrated and comprehensive analysis of fusion, resonance and scattering data in the best studied case of $^{12}C+^{12}C$ reaction within the framework of optical potential model.

Keywords. Optical model potential; heavy ion fusion; resonances; scattering; $^{12}C+^{12}C$ system.

PACS Nos 25.70.-z; 25.70.Ef; 25.70.Bc

1. Introduction

Over the years, extensive experimental as well as theoretical works have been carried out for the process of fusion besides elastic scattering and resonance phenomena in the case of $^{12}C+^{12}C$ system [1–6]. The large amount of measured data of fusion cross-section ($\sigma_{\rm fus}$) [1,2,7] over a wide range of energy can be set in three regions: (I) 2–6 MeV, (II) 6–26 MeV and (III) 26–60 MeV. With reference to the Coulomb barrier $V_{\rm B} \approx 6$ MeV in this system, the regions I, II and III can be termed as sub-barrier, above barrier and high energy regions, respectively. In each of these regions, we find some important features in the results of $\sigma_{\rm fus}$. The region I shows oscillation in the form of cross-section factor $S = E_{\rm cm}\sigma_{\rm fus}\exp(2\pi\eta)$ and draws attention in the astrophysical studies [2,7]. Here, $E_{\rm cm}$ and η stand for incident center of mass energy and Sommerfeld Coulomb parameter, respectively. Region II also shows

oscillation in $\sigma_{\rm fus}$ with 3–4 distinct peaks at $E_{\rm cm} \approx 10$, 14, 21 and 26 MeV [1]. In region III, we find that $\sigma_{\rm fus}$ decreases with further increase of $E_{\rm cm}$ [1].

The measurements for resonance energy in the ^{12}C+^{12}C reaction record several resonances in specific orbital angular momenta [4] and they are usually considered as nuclear molecular resonances in the literature [8].

A natural way to analyze these data is the microscopic coupled channel (CC) calculation besides many macroscopic models developed for specific events. However, there is hardly any approach which is fully successful in explaining the data of fusion, resonance and scattering processes in one platform. In this paper, we address these three phenomena of ^{12}C+^{12}C reaction in a coherent manner within the framework of optical model.

In the conventional compound nucleus model for fusion, the nuclear reaction is visualized in two steps: penetrating first, then decaying. Once the outside barrier is transmitted through, fusion or compound nucleus is assumed to be inevitable. Based on this concept, the well-known barrier transmission model [9] and its improvement over the years [10–12] are seen to be quite remarkable in the analysis of heavy ion (HI) fusion data. Even the more microscopic CC calculation [13] is based on this idea adopted in terms of imposing a boundary condition on the incoming wave. However, these models of fusion may not be applicable to fusion of light nuclei like ^{12}C+^{12}C, because the penetrating particle may still remember its phase factor of the wave function. In this situation, the selective resonant tunneling (SRT) model for fusion presented by Li *et al* [14] is quite interesting. In this model, $\sigma_{\rm fus}$ is considered as part of the total reaction cross-section ($\sigma_{\rm r}$) in the presence of resonances. A weakly absorbing potential used in the analysis of nucleus–nucleus reaction involving light nuclei such as ^{12}C+^{12}C, is found to generate resonance states. The energy of these resonances can be correctly determined by the position of the peaks in the variation of $\sigma_{\rm r}$ with incident energy E [15]. The magnitude of the peak of $\sigma_{\rm r}$ at a given resonance energy critically depends upon the imaginary part W of the potential responsible for reaction or absorption. There is an optimum value of W to give maximum $\sigma_{\rm r}$ at a given resonance. That is, the manifestation of a resonance in reaction cross-section is destroyed if the value of W used is away from this optimum value. Sharper resonance requires small W and broader resonance requires large W for their full manifestation. In a real potential having a pocket and a barrier, the resonances at lower energies are sharper and those in the higher energy region are broader. As different resonances require different W, one has to consider an energy-dependent $W(E)$ for their simultaneous manifestation in the plot of $\sigma_{\rm r}$ with E over a wide range. Thus, the results of $\sigma_{\rm r}$ can be controlled by $W(E)$ where some resonance peaks can be suppressed and some other can be enhanced. The results of $\sigma_{\rm r}$ thus selected by a suitable choice of energy-dependent $W(E)$ can be taken as $\sigma_{\rm fus}$ to account for the corresponding experimental data. For the analysis of $\sigma_{\rm fus}$ data in the case of ^{12}C+^{12}C system, we use this concept of fusion and explain the oscillatory structure in these data quite convincingly reproducing most of the prominent peaks. Further, in the high energy region III mentioned earlier, the results of $\sigma_{\rm fus}$ dropping down with energy can be explained correctly by a $W(E)$ which is decreasing with energy. Further, through dispersion relation, $W(E)$ gives rise to some amount of energy-dependent real potential called polarization potential which is to be included in the real part of the OMP.

Further, the values of $\sigma_{\rm fus}$ in the sub-barrier region I is presented in the form of astrophysical S-factor. The corresponding measured data [2,7] are found oscillatory in nature and our calculated results are good enough to account for these data. In this analysis, we find the necessity of incorporating a soft repulsive core in the real part of the OMP. In order

to do this one may add a term $V_1\exp(-\alpha r)$ to the usual Woods–Saxon form for the nuclear part of the potential with two extra parameters V_1 and α as is done in [2]. However, in our present analysis we found it convenient to represent the nuclear potential by a new form which has an in-built repulsive core. Using this form of potential along with the Coulomb part and polarization potential obtained from dispersion relation, we analyze the elastic differential scattering cross-section at some given energies. Having obtained a reasonable fit to the measured data, particularly in the forward angles, we proceed to the analysis of fusion and resonance data using the same potential. The fits to the elastic scattering data are improved by incorporating a distortion potential in the surface region.

Using the same potential which explain the fusion and scattering data, all possible resonance states in specific partial waves are searched. We find twenty such resonances and on comparison, some of them are found close to the experimentally observed resonances in $^{12}C+^{12}C$ [16,17]. The resonances which are not reproduced by the present approach may not be simple potential resonances.

The paper is organized in the following way. In §2, we describe the OMP with a new form of nuclear potential including energy-dependent imaginary part, dispersion relation and the coupling term. We outline the concept of selective resonance tunneling for fusion in §3. In §4, we present the numerical results and explanation of the respective measured data. Section 5 contains the summary and conclusions.

2. Optical model potential

In the study of elastic scattering, fusion, etc. in nucleus–nucleus collision the phenomenological optical model potential (OMP) has the general form

$$U(r) = V(r) + iW(r), \tag{1}$$

where $V(r)$ and $W(r)$ are the real and imaginary parts of the complex potential $U(r)$. When the potential is used in the radial Schroedinger equation, the effective potential governing the radial motion becomes

$$U_{\text{eff}}(r,l) = V(r) + iW(r) + U_{\text{C}}(r) + \frac{l(l+1)h^2}{2mr^2}. \tag{2}$$

The most commonly used form for $V(r)$ and $W(r)$ is the Woods–Saxon form given as

$$V(r) = -V_0\, g(R,a,r) = -V_0\left[1+\exp\left(\frac{r-R}{a}\right)\right]^{-1} \quad \text{with} \quad R = r_0(A_1^{1/3}+A_2^{1/3}), \tag{3}$$

$$W(r) = -W_0 g(R_I,a_I,r) = -W_0\left[1+\exp\left(\frac{r-R_I}{a_I}\right)\right]^{-1} \quad \text{with} \quad R_I = r_I(A_1^{1/3}+A_2^{1/3}), \tag{4}$$

where the depth parameters V_0 and W_0, radius parameters r_0 and r_I and the diffuseness parameters a and a_I are the six OMP parameters. A_1 and A_2 are the mass numbers of the colliding particles having corresponding proton numbers Z_1 and Z_2. Similarly one uses the following expression for the Coulomb potential:

$$U_{\mathrm{C}}(r) = \begin{cases} \frac{Z_1 Z_2 e^2}{2R_{\mathrm{C}}^3}(3R_{\mathrm{C}}^2 - r^2), & \text{if } r \le R_{\mathrm{C}} \\ \frac{Z_1 Z_2 e^2}{r}, & \text{if } r > R_{\mathrm{C}} \end{cases}, \tag{5}$$

where $R_{\mathrm{C}} = r_{\mathrm{C}}(A_1^{1/3} + A_2^{1/3})$ and r_{C} is the Coulomb radius parameter. The last term in the expression (2) is the centrifugal energy term with l denoting partial wave and m is the reduced mass of the two colliding nuclei having masses m_1 and m_2.

In this paper we introduce a new form for the real part $V(r)$ which is expressed as

$$V(r) = -\begin{cases} V_1 - (V_1 - V_2)\rho_1(r), & \text{if } r \le \overline{R} \\ V_2\rho_2(r), & \text{if } r > \overline{R} \end{cases}, \tag{6}$$

where $\rho_n(r) = [\cosh^2 \frac{r-\overline{R}}{d_n}]^{-1}$, $n = 1, 2$. Here the depth parameters are $V_1 > 0$ and $V_2 > 0$ and they decide the depths of the potential near the origin $r = 0$ and at the pocket position $r = \overline{R}$, respectively. The slopes of the potential on either side of the pocket position are controlled by the slope parameters d_1 and d_2. For $V_1 < V_2$, we get a repulsive core near the origin, whereas for $V_1 = V_2$ the form of the potential is similar to a Woods–Saxon form discussed earlier. This is an exactly solvable potential for s-wave and it readily provides an in-built soft repulsive core as required in various calculations [2], unlike the simple attractive Woods–Saxon form factor.

Further, in heavy-ion scattering a distortion potential is generated in the surface region due to the effects of coupling interaction and adiabatic transfer amongst different channels [5]. Such a distortion or coupling potential can be represented by the double derivative of the Woods–Saxon form of nuclear potential as recently done in ref. [18]:

$$V_{\mathrm{coup}}(r) = -\frac{V_{\mathrm{cp}}}{a_{\mathrm{cp}}^2}\frac{F(F-1)}{(1+F)^3}, \tag{7}$$

where $F = \exp((r - R_{\mathrm{cp}})/a_{\mathrm{cp}})$. The parameters V_{cp}, a_{cp} and $R_{\mathrm{cp}} = r_{\mathrm{cp}}(A_1^{1/3} + A_2^{1/3})$ represent strength, diffuseness and range, respectively. This additional coupling term being added to the nuclear part (6) changes the shape of the conventional Coulomb barrier and improves the explanation of elastic scattering cross-section data significantly.

Recent works on OMP analysis [13,19] point out that there is a rapid variation of the real $V(r)$ and imaginary $W(r)$ parts of the OMP with the incident energy E in the vicinity of the Coulomb barrier. We introduce the energy dependence of the potential along the line suggested in ref. [19]. The general expression for energy-dependent OMP can be written as

$$U(r,E) = V(r,E) + iW(r,E), \tag{8}$$

where the real part $V(r,E)$ can be expressed as a sum of two terms

$$V(r,E) = V(r) + \Delta V(r,E). \tag{9}$$

The energy-independent part $V(r)$ can be expressed as (6). The energy-dependent correction term $\Delta V(r,E)$ very often called as polarisation potential can be obtained from the energy-dependent imaginary part $W(r,E)$ using dispersion relation. We factorize $W(r,E)$ as

$$W(r,E) = -W_0(E) g(R_I, a_I, r), \tag{10}$$

where $g(R_I, a_I, r)$ is the radial form factor same as that in eq. (4). The energy-dependent depth parameter $W_0(E)$ of the imaginary part can be taken in various forms as a function of energy [20]. In this paper we use a linear segment (LS) form. In the LS form, we take an expression consisting of three linear segments given as

$$W_0(E) = \begin{cases} W_1, & \text{if } E < E_a \\ \frac{W_1(E_b-E)+W_2(E-E_a)}{E_b-E_a}, & \text{if } E_a < E < E_b \\ \frac{W_2(E_c-E)+W_3(E-E_b)}{E_c-E_b}, & \text{if } E_b < E < E_c \\ \frac{W_3(E_m-E)}{E_m-E_c}, & \text{if } E_c \le E \le E_m \\ 0, & \text{if } E > E_m \end{cases} . \tag{11}$$

Here W_1, W_2 and W_3 are the depth parameters and they are positive quantities. E_a, E_b, E_c and E_m are the energy parameters at the ends of the segments.

We further assume that the polarization potential $\Delta V(r,E)$ can be written as a product of two factors:

$$\Delta V(r,E) = \Delta V(E)\ f_{\Delta V}(r). \tag{12}$$

The energy-dependent correction term $\Delta V(E)$ can be calculated from the dispersion relation

$$\Delta V(E) = (E - E_g)\left(\frac{1}{\pi}\right) P \int_0^\infty \frac{W_0(E')}{(E'-E_g)(E'-E)} \mathrm{d}E', \tag{13}$$

where P denotes the principal value of the Cauchy integral and E_g is a reference energy which lies in the energy domain of interest.

Using the LS form of $W_0(E)$ given by expression (11), we obtain

$$\begin{aligned} \Delta V^{(\mathrm{LS})}(E) = {} & \frac{(W_2-W_1)}{\pi}\left[\frac{E-E_a}{\Delta_1}\log\left|\frac{E-E_a}{\Delta_1}\right| - \frac{E-E_b}{\Delta_1}\log\left|\frac{E-E_b}{\Delta_1}\right|\right] \\ & + \frac{(W_3-W_2)}{\pi}\left[\frac{E-E_b}{\Delta_2}\log\left|\frac{E-E_b}{\Delta_2}\right| - \frac{E-E_c}{\Delta_2}\log\left|\frac{E-E_c}{\Delta_2}\right|\right] \\ & - \frac{W_3}{\pi}\left[\frac{E-E_c}{\Delta_m}\log\left|\frac{E-E_c}{\Delta_m}\right| - \frac{E-E_m}{\Delta_m}\log\left|\frac{E-E_m}{\Delta_m}\right|\right] \\ & + \frac{W_3}{\pi}[(1+\eta)\log(1+\eta) - \eta\log\eta]. \end{aligned} \tag{14}$$

Here, $\Delta_1 = E_b - E_a$, $\Delta_2 = E_c - E_b$, $\Delta_m = E_m - E_c$ and $\eta = \Delta_2/\Delta_m$.

This energy-dependent correction term is to be added to the nuclear potential. Assuming the radial form $f_{\Delta V}(r)$ to be same as that of $V(r)$ and replacing V_2 by $V_2 + \Delta V(E)$ in eq. (6) we obtain the necessary energy-dependent real part of OMP.

In figure 1a, we show the variation of $W(r,E)$ with energy at a given radial distance $r = 6.3$ fm using the LS (solid line) form for $W_0(E)$ given by expression (11). The corresponding variation of $V(r,E) = V(r) + \Delta V(r,E)$ with energy $E = E_{\mathrm{cm}}$ are shown in the

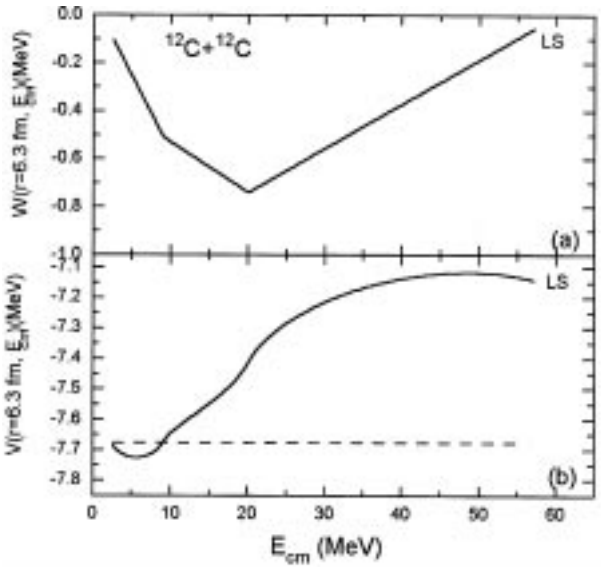

Figure 1. (**a**) Variation of imaginary potential $W(r, E_{\rm cm})$ as a function of incident center-of-mass energy $E_{\rm cm}$ at the position $r = 6.3$ fm for ^{12}C+^{12}C reaction. Solid line is for LS form given by eq. (11) described in the text. (**b**) Variation of real part $V(r, E_{\rm cm}) = V(r) + \Delta V(r, E_{\rm cm})$ with energy. Solid line is for LS form. The dashed line represents constant value of $V(r)$ at $r = 6.3$ fm.

figure 1b by a solid line. The dashed horizontal line indicates the constant value of $V(r)$ at $r = 6.3$ fm.

In order to show the energy dependence of the real effective potential, we plot in figure 2 the variation of real part of the total effective potential $U_{\rm eff}(r, E)$ as a function of r for $l = 0$ at three different incident energies above and below the Coulomb barrier. It is clearly seen that the height of the potential near the barrier is not changed much whereas the potential is significantly changed near the pocket region. Figures 1 and 2 demonstrate the nature of the real part of OMP that we use in our analysis.

3. Selective resonance tunneling

Using the complex optical potential described in the previous section, we solve the Schroedinger equation numerically and find the scattering matrix (S_l) for each l. The reaction cross-section $\sigma_{\rm r}$ is expressed as

$$\sigma_{\rm r} = \sum_{l=0}^{\infty} \sigma_{\rm r}^{l}, \tag{15}$$

$$\sigma_{\rm r}^{l} = \frac{\pi}{k^2}(2l+1)T_l, \tag{16}$$

$$T_l = 1 - |\, S_l \,|^2, \tag{17}$$

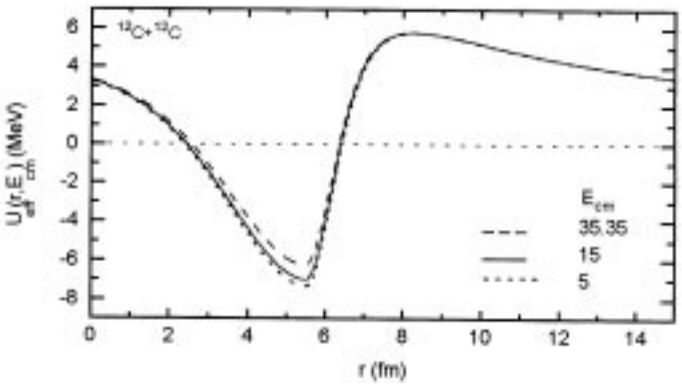

Figure 2. Plot of real effective potential $U_{\rm eff}(r, E_{\rm cm})$ as a function of radial separation r at $E_{\rm cm} = 35.35$ MeV (dashed curve), $E_{\rm cm} = 15$ MeV (solid curve) and $E_{\rm cm} = 5$ MeV (dotted curve). The potentials correspond to $l = 0$ for ^{12}C+^{12}C system.

where T_l is a measure of transmission probability contributing to fusion for a given partial wave l and $\sigma_{\rm r}^l$ indicates the partial wave reaction cross-section. One can write T_l in a different form as follows: We have $S_l = \exp(2i\delta_l)$, where δ_l is the total phase shift and it is complex due to the complex OMP. Presenting δ_l in the form [14] $\cot\delta_l = Z_r + iZ_i$, we get

$$T_l = \frac{-4Z_{\rm i}}{Z_{\rm r}^2 + (Z_{\rm i} - 1)^2}. \tag{18}$$

In potential scattering, there are many ways to determine the energies at which the system resonates. In one of these methods, one may consider the positions of peaks in the variation of $\sigma_{\rm r}^l$ with the bombarding energy as resonance energies. In other words, the energy positions of the maxima of the transmission probability T_l can be taken as resonance energies [14]. T_l reaches its maximum when

$$\begin{cases} Z_{\rm r} = 0 \\ Z_{\rm i} = -1 \end{cases}. \tag{19}$$

Evidently, $Z_{\rm r} = 0$ corresponds to the condition for resonance [14]. On the other hand, $Z_{\rm i}$ is related to the imaginary part $W(r,E)$ of the OMP. Clearly, if $W(r,E) = 0$, the phase shift is real and we get $Z_{\rm i} = 0$ which gives $T_l = 0$. Further, as demonstrated in ref. [14], even at the resonance, the transmission probability and hence $\sigma_{\rm r}$ is very small if W is too large or too small. That is, there is an optimum value of $\mid W \mid$ for making $T_l = 1$ at the resonance. Further, it is known that the width of the resonance is of the order of $\mid W \mid$ as the lifetime of the compound state inside the nuclear cell is $\tau \sim \hbar/\mid W \mid$.

As a natural understanding of compound nucleus formation, one may take part of $\sigma_{\rm r}$ as the fusion cross-section $\sigma_{\rm fus}$ [19]. In view of the above link of resonance phenomenon with the partial wave reaction cross-section, the results of $\sigma_{\rm fus}$ will certainly be governed by the resonance phenomena. In the case of a given l, if there are more than one resonance states, a constant value for $\mid W \mid$ may be favorable to one of them when the other states are suppressed. Hence, to extract the fusion cross-section it is necessary to use an appropriate energy-dependent optical potential which can manifest the effect of resonances and identify

Table 1. Values of parameters for the energy-dependent OMP for fusion: (a) for real part $V(r)$ (eq. (6)) and $V_C(r)$; (b) for imaginary part $W(r,E)$ in the LS form (eq. (11)); (c) for coupling term (eq. (7)) with $V_C(r)$.

(a)

V_1 (MeV)	V_2 (MeV)	d_1 (fm)	d_2 (fm)	$\overline{R}$ (fm)	r_C (fm)
3.5	14.8	2.9	1.07	5.45	1.6

(b)

Set	W_1 (MeV)	W_2 (MeV)	W_3 (MeV)	a_I (fm)	r_I (fm)	E_a (MeV)	E_b (MeV)	E_c (MeV)	E_m (MeV)
I	0.01	0.62	0.9	0.49	1.53	2	9	20	60

(c)

V_{cp} (MeV)	a_{cp} (fm)	r_{cp} (fm)	r_C (fm)
1.0	0.2	1.35	1.6

the reaction cross-section generated by it as fusion cross-section. Needless to say, this fusion cross-section will be less than or equal to the corresponding reaction cross-section generated by the full optical potential describing scattering cross-section.

4. Numerical results and discussion

We calculate the results of fusion cross-section σ_{fus}, astrophysical S-factor, differential scattering cross-section ($d\sigma/d\Omega$) and resonances in specific trajectories in the case of $^{12}C+^{12}C$ system which is an important case of light–heavy-ion reaction. The values of the energy-dependent OMP and coupling parameters used in the present calculation are listed in table 1.

4.1 *Oscillation in fusion cross-section*

In figure 3, we present our calculated results of σ_{fus} as a solid curve for bombarding energy $E_{cm} = 7$–34 MeV. These results are compared with the corresponding experimental data (solid dots) taken from [1]. As is clearly seen, the oscillatory structure in the measured data is explained satisfactorily by our calculated results. The important peaks in the experimental data near $E_{cm} = 14$, 21 and 26 MeV are nicely shown by the solid curve. However, two more prominent peaks near 9 MeV and 11 MeV shown by the solid curve do not find measured data in this figure 3 matching with them. But, other experimental works [17] confirm the presence of these peaks in the measured data along with several other peaks in

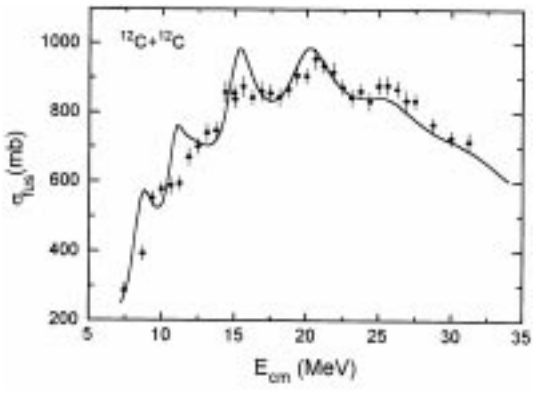

Figure 3. Variation of fusion cross-section $\sigma_{\rm fus}$ as a function of $E_{\rm cm}$ for the ^{12}C+^{12}C system. The solid curve represents the calculated results. The solid dots representing corresponding experimental data are obtained from ref. [1].

the energy range $E_{\rm cm} = 7$–20 MeV. However, the overall magnitude of this experimental fusion cross-section data [17] is found to be smaller than those shown in figure 3. Using a smaller value of the strength of the imaginary part, we obtain our calculated results which can explain these data from [17] in terms of average magnitude as well as prominent peaks. It may be pointed out here that the smooth continuous curve shown along with the data in ref. [1] is not based on theoretical calculations, but has been drawn to guide the eyes [1]. Our aim is to fit in an optimal manner the experimental data available on $\sigma_{\rm fus}$ [1] and elastic scattering $\mathrm{d}\sigma/\mathrm{d}\sigma_{\rm C}$ and in this process some sections of the resonance data get somewhat overestimated in height, but peak positions are retained.

Further, in figure 3, we see that in the higher energy region ($E_{\rm cm} > 20$ MeV) the $\sigma_{\rm fus}$ data show decreasing trend and this is also nicely accounted for by our calculated results shown by the solid curve.

4.2 *Fusion cross-section S-factor*

In the sub-barrier region of energy $E_{\rm cm} < V_{\rm B} = 5.8$ MeV, $\sigma_{\rm fus}$ can be analyzed in the form of cross-section factor $S = E_{\rm cm}\sigma_{\rm fus}\exp(2\pi\eta)$, where η is the Sommerfeld–Coulomb parameter. For the ^{12}C+^{12}C reaction, $2\pi\eta = 2\pi Z_1 Z_2 e^2/\hbar v = 87.2/\sqrt{E_{\rm cm}(\mathrm{MeV})}$. Usually, $\sigma_{\rm fus}$ is studied in this form in nuclear astrophysics. In figure 4, we compare the experimental data of the *S*-factor with our calculated results represented by a solid curve. There are two sets of measured data shown in this figure in 10^{15} MeV barn unit. Data indicated by solid circles are taken from [2] and those from [7] are shown by open squares. As seen, these data, like $\sigma_{\rm fus}$ in the above barrier region, show oscillatory structure and our calculated results explain this trend convincingly. Our calculated results generally fall in between the data points obtained by High *et al* [2] and Patterson *et al* [7]. This is remarkable in view of the fact that the earlier calculated results of *S*-factor [2,19] fail to exhibit this oscillatory structure. In our *S*-factor calculations, we use a soft repulsive core for the nuclear part of the OMP through the expression (6). Similar repulsive core was used in ref. [2] but with

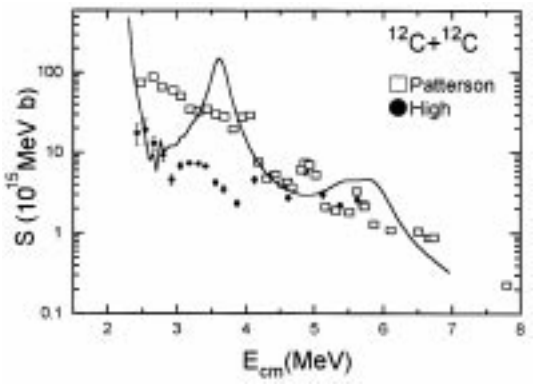

Figure 4. Energy dependence of the astrophysical *S*-factor for $^{12}C+^{12}C$ reaction. The solid curve represents the calculated results. The experimental data indicated by solid circles are taken from ref. [2] and those indicated by open squares are from ref. [7].

an exponential form. We find that a repulsive core is very essential to account for the experimental results of *S*-factor particularly in the very low energy region (2–3 MeV). Thus, fusion data at very low energy can be used to probe phenomenologically the nature of the potential in the interior region near the origin. This is important due to the fact that elastic scattering data are not sensitive to the potential in the deep interior side of the Coulomb barrier.

4.3 *Elastic scattering cross-section*

Having obtained a satisfactory explanation of the fusion data over a wide range of energy including the *S*-factor, the OMP used in the calculation is tested for the analysis of elastic scattering data at some energies. In the phenomenological analysis, it is well-known that the folding model with a deep potential is best suited for the analysis of differential scattering cross-section ($d\sigma/d\Omega$) as a function of center-of-mass angle θ_{cm} at given energies in the case of systems like $^{12}C+^{12}C$ [3,6]. Even in such calculations, one has to change the potential at each energy to give a best fit to the data. On the other hand, a shallow OMP in the Woods–Saxon form is successful in forward angles only [3]. Our potential given by expression (6) along with the parameters listed in table 1 is a potential in this category and hence, we calculate ($d\sigma/d\Omega$) to fit the data in the forward angular region. The coupling potential given by (7) with its parameters listed in table 1c is added to the nuclear part given by equation (6). In figure 5, our calculated results are represented by the solid curves. In this figure, we compare these calculated results of differential scattering cross-section normalized to Coulomb cross-section as a function of center-of-mass angles at several energies near the Coulomb barrier with the corresponding experimental data obtained from ref. [16]. As is clearly seen, our results are close to the respective measured data in the forward angular region. It may be mentioned here that similar fitting to the elastic scattering data can be obtained if one uses an energy-independent, highly absorptive and too deep OMP as done in ref. [16]. But, such a potential is not able to address the oscillatory structure found in the measured σ_{fus} data in the case of $^{12}C+^{12}C$ system.

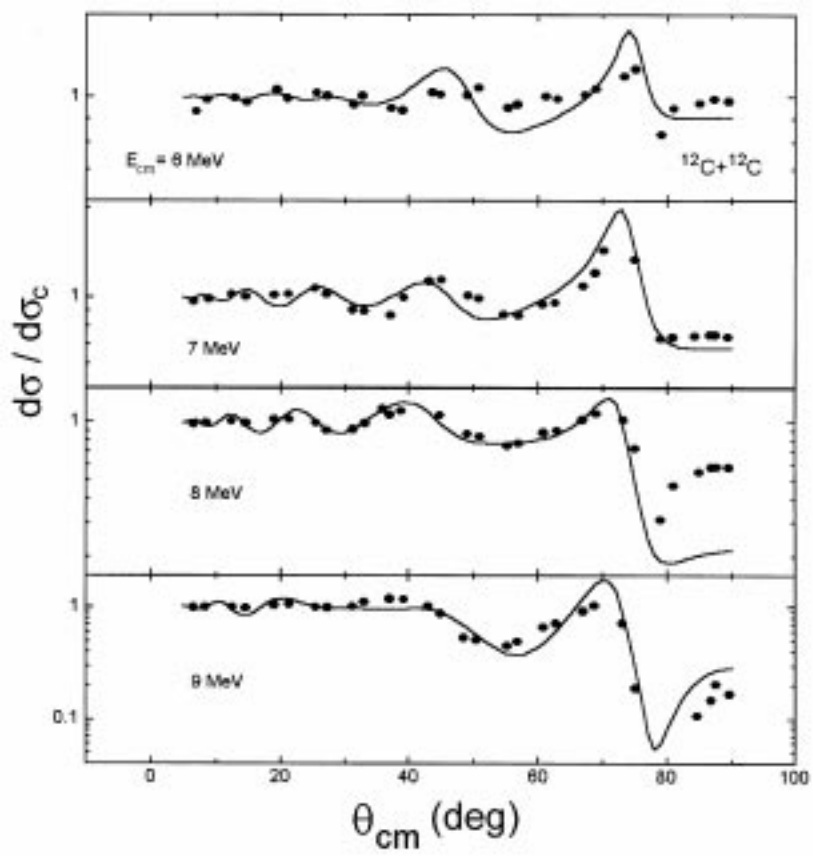

Figure 5. Angular distribution of elastic scattering of $^{12}C+^{12}C$ normalized to Coulomb cross-section. Calculated results are shown by solid curves. The experimental data points are obtained from ref. [16].

Thus, we have succeeded in explaining $^{12}C+^{12}C$ fusion data and forward region scattering data in an integrated way within the framework of optical model using a repulsive potential near the origin, a coupling or distortion potential near the surface and the polarization potential obtained from the dispersion relation between real and imaginary parts of the potential originated from the energy-dependent imaginary attractive potential. Hence, it is important to see if this potential can generate at least a part of the set of resonances experimentally identified in $^{12}C+^{12}C$ system thereby linking the resonances with σ_{fus} oscillation. This we discuss in the next sub-section.

4.4 *Resonances generated by $^{12}C+^{12}C$ fusion potential*

To correlate the fusion cross-section σ_{fus} for $^{12}C+^{12}C$ system with the corresponding resonances, it is appropriate to identify the resonances generated through the peaks of the partial wave reaction cross-section σ_r^l as σ_{fus} is taken as part of the total reaction cross-

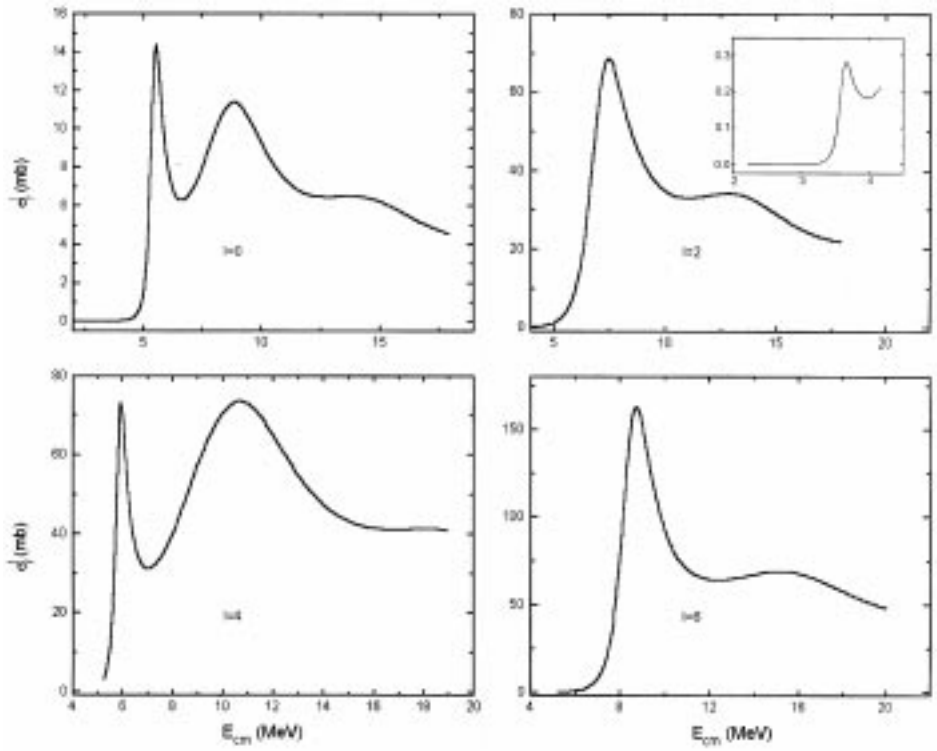

Figure 6. Variation of partial wave reaction cross-section σ_r^l as a function of E_{cm} for $l = 0, 2, 4$, and 6 in $^{12}C+^{12}C$ reaction. The strength of the imaginary part W_0 used in this calculation is same as that used in the calculation of σ_{fus} (see table 1).

section σ_r. It is shown in ref. [15] that it is easier to locate and identify the resonances generated by a potential through σ_r^l rather than elastic cross-section because the former does not manifest non-resonant peaks generated by echoes and shape resonances. Experimental fusion cross-section will contain the contributions from all partial waves and hence it is not easy to locate resonance positions from the σ_{fus} data. Hence, each partial wave needs to be examined carefully for the presence of resonance. We calculate $\sigma_r^l = \frac{\pi}{k^2}(2l+1)(1-|S_l|^2)$ and study its variation as a function of incident energy. As stated above and also in our recent paper [21], the energy positions of these peaks in this plot represent resonance energies. In figures 6, 7 and 8, we illustrate the variation of σ_r^l for all even ls in the range $l = 0$–18 where the strength of the imaginary part considered is same as that used for the calculation of σ_{fus}. From this calculation we obtain about 20 resonances from different ls which are listed in table 2. About 15 of these resonances are found to be very close to the experimentally identified resonances in $^{12}C+^{12}C$ reaction where about 31 such resonances are reported in [17]. Hence, we may say that at least a substantial sub-set of $^{12}C+^{12}C$ resonances are potential resonances which can be incorporated in the optical potential.

Having the optical potential constructed to generate the fusion and scattering data we find that one can obtain a number of $^{12}C+^{12}C$ resonances even though many resonances found in experimental data are not generated by our potential. This should not be surprising

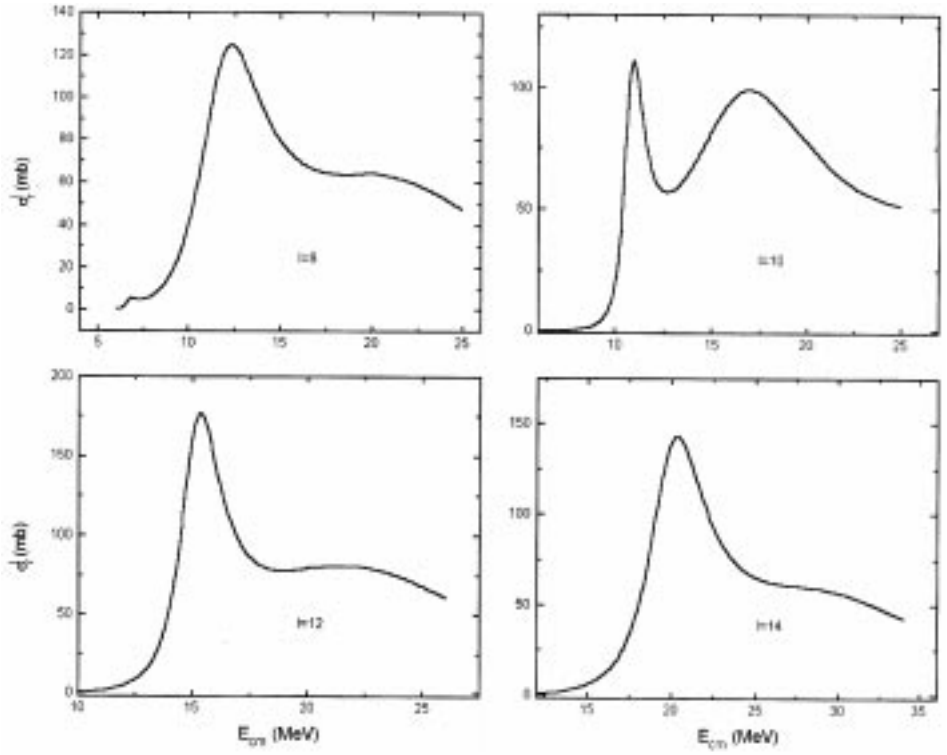

Figure 7. Same as figure 6 for $l = 8$, 10, 12, and 14.

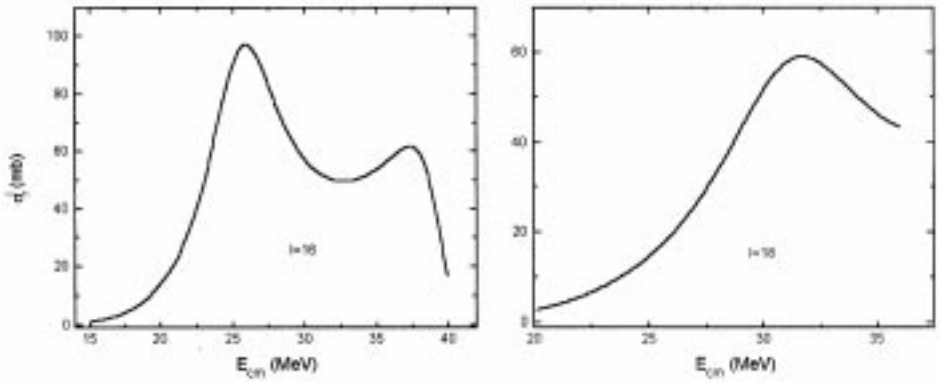

Figure 8. Same as figure 6 for $l = 16$ and 18.

because it is too simplistic to expect that in the complex $^{12}C+^{12}C$ collision all resonances generated will be potential resonances. Nevertheless, our calculations here give an integrated picture of fusion, resonances and scattering in the case of $^{12}C+^{12}C$ reaction.

Table 2. Resonances observed $^{12}C+^{12}C$ reaction.

l	E_{cm} (MeV)	l	E_{cm} (MeV)
0	2.3	10	10.95
	5.55		17.0
	8.5		
	13.8		
2	3.65	12	15.37
	7.5		
	12.8		
4	5.95	14	20.35
	10.70		
6	8.70	16	25.88
	15.15		37.32
8	6.90	18	31.70
	12.35		

5. Summary and conclusions

The processes of fusion, resonances and elastic scattering in the $^{12}C+^{12}C$ reaction are investigated together. A close look at the experimental results of fusion cross-section σ_{fus} in this case reveals that the results as a function of incident energy are oscillatory around the Coulomb barrier energy and show a decreasing trend in the very high energy region. Further, this reaction sustains many prominent resonances in specific partial waves l. We analyze these data within the framework of optical model potential (OMP) scattering and reaction. In a nucleus–nucleus collision involving light–heavy ions such as $^{12}C+^{12}C$, $^{12}C+^{16}O$ etc. one finds a number of resonances around the barrier. The OMP used in the analysis of such systems is generally weakly absorbing and in principle capable of generating at least a sub-set of observed resonances. The energy of a resonance state for a given partial wave l can be identified from the position of the peaks in the plot of partial wave reaction cross-section σ_r^l with the bombarding energy. It is seen that the magnitude of a peak at the resonance depends critically upon the imaginary part W of the potential used in the OMP. Values of W too large or too small destroy the peak of the resonance. Hence, by using an energy-dependent W in the OMP we can control and select the values of σ_r^l at different energies. Adopting the concept that fusion is part of the reaction process, we use suitable W to calculate σ_r and identify this with the fusion cross-section σ_{fus}. This method of estimating σ_{fus} to include resonance effects may be termed as 'selective resonance tunneling' (SRT). In the process of doing this, we find that the energy-dependent $W(E)$ gives rise to energy-dependent real potential through the dispersion relation. This is properly incorporated in the main bulk of real part of the OMP. In the present calculation, instead of the Woods–Saxon form, we introduce a new form of potential for the nuclear part with a soft repulsive core in-built in it which is found necessary to generate the astrophysical S-factor. Based on this approach, we obtain the oscillatory structure in the measured results of fusion cross-section $\sigma_{fus}^{(expt)}$ [1] correctly with all the prominent peaks in phase.

Further, the decreasing values of $\sigma_{\rm fus}^{(\rm expt)}$ in the high-energy region are accounted for by our calculated $\sigma_{\rm fus}$ where a decreasing $\mid W \mid$ with energy is found essential.

In the sub-barrier region of energy $E_{\rm cm} = 2$–6 MeV, the results of $\sigma_{\rm fus}^{(\rm expt)}$ presented in the form of cross-section factor S in astrophysical studies, are also found oscillatory and they are explained with close proximity by the corresponding results of the present calculation. In this analysis, we find that a repulsive soft core in the potential near the origin is highly essential. This result indicates that fusion cross-section data can be used to predict the nucleus–nucleus potential close to origin unlike the elastic scattering data which are sensitive in the surface region only.

The potential used to estimate $\sigma_{\rm fus}$ is tested for the analysis of differential scattering cross-section ($\mathrm{d}\sigma/\mathrm{d}\Omega$) data at some given energies. The scattering data are fitted well particularly in the forward angular region. By incorporating a coupling potential effective in the surface region the explanation of the elastic data is improved. We then search all the resonances generated by the potential used for fusion in different ls. We find around twenty such resonances and, on comparison, fifteen are found to be close to experimentally identified resonances reported in [16,17] where about 31 resonances are listed for the $^{12}C+^{12}C$ system. The resonances which are not reproduced by our potential are likely to belong to the processes which are more microscopic in nature.

In conclusion, we may mention that in the nucleus–nucleus collision involving light–heavy ions where weakly absorbing potential is generally used, selecting a part of the total reaction cross-section with the help of an energy-dependent imaginary potential in the OMP, one can account for the experimental results of fusion cross-section with their oscillatory structure over a wide range of energy. As the weakly absorbing potential generate resonances and the resonances can be identified through peaks in the reaction cross-section, one can clearly understand the influence of resonances in the process of fusion in the $^{12}C+^{12}C$ system. Thus, the oscillatory structure in $\sigma_{\rm fus}$ is found to be linked to the resonant behavior of the system in specific partial wave trajectories. Application of this theory to other light–heavy ion reactions is in progress.

Acknowledgement

We are thankful to Prof. L Satpathy for valuable discussion. BS acknowledges the support of DST, New Delhi vide Research Grant No. SP/S2/K14/96(PRU) and BRNS, Mumbai vide Research Grant No. 2000/37/11/BRNS/704.

References

[1] D G Kovar *et al*, *Phys. Rev.* **C20**, 1305 (1979)
[2] M D High and B Cujec, *Nucl. Part. Phys.* **A282**, 181 (1977)
[3] R M Wieland, R G Stokstad, G R Satchler and L D Rickertsen, *Phys. Rev. Lett.* **37**, 1458 (1976)
[4] N Cindro, *Riv. Nuovo Cimento* **4**, 1 (1981)
[5] O Tanimura and T Tazawa, *Phys. Rep.* **61**, 253 (1980)
[6] G R Satchler, in *Proc. Sixth INS Summer School on Nuclear Physics* (Dogasima, Japan, 1978)
[7] J R Patterson, H Winkler and C S Zaidins, *Astrophys. J.* **157**, 367 (1969)
[8] L Satpathy, *Prog. Part. Nucl. Phys.* **29**, 327 (1992)

[9] D L Hill and J A Wheeler, *Phys. Rev.* **89**, 1102 (1953)
[10] T Udagawa, B Kim and T Tamura, *Phys. Rev.* **C32**, 124 (1985)
[11] B Sahu and C S Shastry, *J. Phys.* **G15**, L149 (1989); **G16**, 55 (1990); **G22**, 1483 (1996); **G25**, 1909 (1999); *Pramana – J. Phys.* **53**, 545 (1999)
[12] B Sahu, I Jamir, E F P Lyngdoh and C S Shasrty, *Phys. Rev.* **C57**, 1853 (1998)
[13] G R Satchler, M A Nagarajan, J S Lilley and I J Thompson, *Ann. Phys.* **178**, 110 (1987)
[14] X Z Li, J Tian, M Y Mei and C X Li, *Phys. Rev.* **C61**, 024610 (2000)
[15] I Jamir, E F P Lyngdoh and C S Shastry, *Pramana – J. Phys.* **50**, 271 (1998)
[16] W Treu, H Frohlich, W Galster, P Duck and H Voit, *Phys. Rev.* **C22**, 2462 (1980)
[17] L J Satkowiak, P A De Young, J J Kolata and M A Xapsos, *Phys. Rev.* **C26**, 2027 (1982)
[18] I Boztosun and W D M Rae, *Phys. Rev.* **C63**, 054607 (2001); *Phys. Rev.* **C64**, 054607 (2001)
[19] J Czakanski *et al*, *Nucl. Phys.* **A580**, 100 (1994)
[20] C Mahaux, H Ngo and G R Satchler, *Nucl. Phys.* **A449**, 354 (1986)
[21] B Sahu, L Satpathy and C S Shastry, *Phys. Lett.* **A303**, 105 (2002)